NASA
Technical
Paper
2921

June 1989

Evaluation of a Strain-Gage Load Calibration on a Low-Aspect-Ratio Wing Structure at Elevated Temperature

Lawrence F. Reardon

NASA

NASA Technical Paper 2921

1989

Evaluation of a Strain-Gage Load Calibration on a Low-Aspect-Ratio Wing Structure at Elevated Temperature

Lawrence F. Reardon
Ames Research Center
Dryden Flight Research Facility
Edwards, California

NASA
National Aeronautics and Space Administration
Office of Management
Scientific and Technical Information Division

CONTENTS

SUMMARY

This report addresses the environmental aspect of elevated temperature and how it relates to the science of strain gage calibrations of aircraft structures. A section of a wing designed for a high-speed aircraft structure was used to study this problem. This structure was instrumented with strain gages calibrated at both elevated and room temperatures.

Load equations derived from a high-temperature load calibration were compared with equations derived from an identical load calibration at room temperature. The implications of the high temperature load calibration were studied from the viewpoint of applicability and necessity. Load equations derived from the room temperature load calibration resulted in generally lower equation standard errors than equations derived from the elevated temperature load calibration. A distributed load was applied to the structure at elevated temperature and strain gage outputs were measured. This applied load was then calculated using equations derived from both the room temperature and elevated temperature calibration data. It was found that no significant differences between the two equation systems existed in terms of computing this applied distributed load, as long as the thermal shifts resulting from thermal stresses could be identified. This identification requires a heating of the structure. Therefore, it is concluded that for this structure, a high temperature load calibration is not required, however, a heating of the structure is required to determine thermal shifts.

INTRODUCTION

Measurement of aircraft loads with calibrated strain gages is a technology that emerged in the 1940s and was presented in a unified approach in 1954 (ref. 1). As aircraft structures, configurations, and environments have changed, additional techniques have been added to the general approach. This report addresses the impact of elevated temperature on the science of strain gage calibrations of aircraft structures. Because the elevated temperature environment can cause material property degradation and the nonuniform temperature distribution in the structure can induce thermal stresses, the validity of applying a room temperature load calibration to a heated structure must be examined.

A section of a wing designed for a high-speed aircraft structure (ref. 2) was used to study this problem. This structure was instrumented with strain gages that were calibrated at both elevated and room temperatures. Resulting load equations were examined to determine the impact of elevated temperatures on the accuracy of the load equations.

NOMENCLATURE

The physical quantities in this report are given in both the International System of Units (SI) and U.S. Customary Units. Measurements were made in Customary Units. Physical constants and conversion factors are given in reference 3.

b	wingspan, m (in.)
c	wing chord, m (in.)
FS	fuselage station
HWTS	hypersonic wing test structure
L	generalized load: shear, bending moment, or torque
T	T-value
WS	wing station
X	axis in chord direction
Y	axis in span direction
β	constant in load equation
ϵ	strain
η	nondimensional span location of the applied load, 2y/b
μ	nondimensional strain gage bridge response
ξ	nondimensional span location of the applied load, x/c

Subscripts:

1,2,3,...,j	order of terms' appearance in load equation
i	discrete function

INSTRUMENTATION AND TEST PROCEDURES

Test Article

The planform of a high-speed airplane and the portion of the wing that is used as a test structure are

shown in figure 1. The test-structure design is based on mission loads and temperatures calculated for the structure concept presented in reference 2. The wing is a complex delta configuration having a planform area of 85 ft^2. The shape and dimensions of the structure with a transition section can be seen in figure 2.

The structure with heat shields installed is shown in figure 3. The wing was cantilevered from wing station (WS) 42 and was tested inverted, so the compressively loaded surface of the actual vehicle was on the lower surface of the test structure. The transition section, which is not part of the aircraft design, was included in the tests to provide a buffer between the support structure and the test portion of the wing.

The structure is primarily constructed of Rene'41 material and has six spars perpendicular to the aircraft centerline. The spar webs and adjoining rib webs have sine wave corrugations to allow for thermal expansion (ref. 2). Spanwise-stiffened, beaded panels cover this substructure. Heat shields are attached to the upper and lower surfaces of the structure with Z-shaped clips. These shields are slightly corrugated in the chordwise direction. Heat shield extensions were also provided around the boundaries of the test structure to improve the simulation of the heating of the outer spar and rib webs.

Instrumentation

Strain Gages

The load measurement instrumentation consisted of 12 four-active-arm strain gage bridges, 6 bending bridges and 6 shear bridges. The strain gages used were a foil type and are located as shown in figure 4.

The bending bridges are configured with two half-bridges, one half-bridge on the upper spar cap and one on the lower spar cap, wired together to form a four-active-arm bridge. Each of the half-bridges is wired in a T configuration to provide temperature compensation. A typical installation of a half-bridge is shown in figure 5(a).

The shear bridges are typically configured at 45° to the X-Y plane and are located on the spar webs midway between the upper and lower spar caps. A typical installation is shown in figure 5(b).

The accuracy of the data acquisition system for strain gage measurements was ±4.88 microstrain, which represents 0.3 percent of the strain gage calibration output.

Thermocouples

Control thermocouples were installed on the heat shield at 14 locations on the upper surface and 10 locations on the lower surface. These thermocouples provided temperature control feedback in 24 zones, as shown in figure 6. Also shown in figure 6 are the locations of 13 monitor thermocouples. These were installed to determine the uniformity of temperatures reached in the zones that heated the strain gages to be calibrated.

Test Setup

Heating System

The test structure was heated using quartz lamps attached to water-cooled aluminum reflectors as shown in figure 7. The heating was controlled using analog temperature control equipment (ref. 4). Temperatures were controlled in 10 zones on the lower heater and 14 zones on the upper heater. This was accomplished by using a control thermocouple located on the heat shield in each zone. The zone and thermocouple arrangements are shown in figure 6.

Since only 24 channels of heating were available for the calibration, the heating zones (fig. 6) are large. These large zones cause difficulty in providing a uniform temperature throughout the zone, because only the control thermocouple location is forced to the programmed temperature. Temperatures at the control and monitor thermocouples in the area of the strain gages indicate this lack of uniformity. The maximum temperatures at the strain gages also indicate this lack of uniformity. The maximum temperatures at the strain gage shear bridges and at the upper and lower halves of the bending bridges are shown in table 1. Heat losses at the edges of the heaters caused the temperatures to drop off approximately 100°F at the forward and aft strain gage locations.

The temperatures shown on figure 6 are maximums reached during the two calibration runs. Figure 6(a) shows the temperatures on the upper portion of the wing. Figure 6(b) shows temperatures reached on the lower portion of the wing.

Loading system

Ten channels of closed-loop electrohydraulic equipment, as described in reference 5, were used to apply vertical loads to the test structure at the locations shown in figure 4. These loads were applied individually for the strain gage calibration. Distributed loads were applied by connecting 16 of the load points with two-point whiffletrees, so that the 10 hydraulic jacks could apply loads at 18 points simultaneously.

Load transducers of various capacities were used to measure the forces applied to the structure. The accuracy of the loading data was governed primarily by the accuracy of these transducers. Inaccuracies from all other sources (for example, jack positioning and the data acquisition system) were considered to be negligible. The estimated accuracy of the load transducers was as follows:

Load transducer capacity, lb	Accuracy, lb
10,000	±25
5,000	±12.5

Further information on the instrumentation and loading equipment may be found in reference 5.

Test Procedure

Original room temperature tests outlined in reference 5 provided the baseline for this study. Three additional tests were performed at elevated temperatures. Two tests using single-point vertical loads applied at different spanwise and chordwise locations were used to calibrate the strain gages, and one test using a set of simultaneously applied single-point loads was used to check load equation accuracy. Locations of the points at which calibration loads were applied is shown in figure 4. Table 2 shows the strain gage calibration loading sequence.

The test structure was heated to and held at 550°F, as measured on the heat shields. Sufficient time was allowed for the internal temperatures to stabilize. (Stabilization was that point at which the internal temperatures had essentially stopped increasing and the strain gage outputs had essentially ceased to change. This technique was used so that any temperature change during loading would have little effect on the output of the strain gages.) Load points 1, 3, 5, 7, 9, 11, 13, 15, 16, and 17 were then loaded individually from zero to 2000 pounds and back to zero (see table 2). The structure was allowed to cool and eight of the jacks were relocated for the final eight points. The structure was reheated, as stated previously, and then points 2, 4, 6, 8, 10, 12, 14, and 18 were loaded in the same manner as the first 10 points.

The elevated temperature check loading was applied at all 18 load points simultaneously. Sixteen of the points were loaded through two-point whiffletrees. This loading results in a midchord center of pressure. The load applied at each point was 2000 pounds.

A similar method of loading was used in the room temperature calibration of reference 6. Data from this calibration are used in the room temperature calculations of this report.

Load Equations

The standard calibration procedure described in references 1 and 8 was used for these tests. Equations expressing the applied loads as linear functions of the corresponding recorded strain gage bridge outputs are derived by solving the following type of matrix equation:

$$L_j = [\mu_{ji}]\{\beta_i\} \qquad (1)$$

where L_j is the jth calibration load, μ_{ji} is the ith strain gage output for the jth calibration load, and β_i is the ith equation coefficient to be determined. The equation coefficients β_i are obtained from equation (1) by regression techniques (least squares estimate of β_i).

The errors involved in performing this analysis (that is, the difference between the calibration load and calculated load using β_i) are calculated as follows (ref. 7):

$$\text{standard error of the equation} = \sqrt{\frac{(L_j - \sum_{i=1}^{n} \mu_{ji}\beta_i)}{m - n}} \qquad (2)$$

where n is the number of strain gages and m is the number of load conditions.

The number of bridges used in an equation can be successfully reduced by use of the T-value method recommended in reference 8 and described in reference 7. T values are defined as

$$T_i = \frac{\beta_i}{\text{standard error of the coefficient}} \qquad (3)$$

where T_i is the T-value and β_i is the equation coefficient. The standard error of the coefficient is obtained as follows (ref. 1):

$$\text{Standard error of the coefficient} = \sqrt{m_{jj}} \qquad (4)$$

where m_{jj} is a diagonal element of a matrix formed from matrix product $[[\mu_{ji}]^T[\mu_{ji}]]^{-1}$. The number of bridges is then reduced by eliminating those with the smallest T-values (irrelevant bridges and redundant bridges). Each time a bridge is discarded, a new equation is derived from the remaining bridges, and new T-values are calculated. This process was used to reduce 12 bridge equations to 2 bridge equations for shear, bending, and torque. The process is also used to examine the accuracy variations of the load equations when reducing the number of bridges in the equation.

Figure 8 shows the increasing error for both the room temperature and elevated temperature cases, as the number of bridges in a load equation is reduced. The smallest errors occur in equations with 12 to 6 bridges. As stated in reference 7, these small errors are procedural errors that include data acquisition errors, load point location errors, and local loading effects.

Equation coefficients β_i were derived for each of the room temperature and elevated temperature load equations.

RESULTS AND DISCUSSIONS

Influence Coefficients

Influence coefficient plots are a concise way of presenting the responses of individual strain gages to a unit applied load as a function of the spanwise and chordwise location. A plot of this nature is useful in determining whether a particular bridge is affected predominantly by shear, bending moment, or torsion loads, by a combination of two, or even by all three.

The influence coefficient plot of a single strain gage bridge, such as the ith bridge, is the variation of the strain per unit load for loads at various spanwise and chordwise locations, and can be expressed as follows:

$$\epsilon_i/L = f_i(\eta, \xi)$$

where ϵ_i is the strain at the ith bridge due to the applied load L, η is the nondimensional spanwise location of the applied load ($\eta = 2y/b$), and ξ is the nondimensional chordwise location of the applied load ($\xi = x/c$).

An ideal shear bridge influence coefficient would have a constant value regardless of the spanwise or chordwise location of the load. This would indicate no response to bending or torque. The ideal plot of bending-bridge influence coefficient as a function of span would take the shape of the load points. Since ideal responses are rare, the influence coefficient plots tend to show the combined effects of shear, bending moment, and torsion loads. Combining strain gage bridges into an equation attempts to create an ideal or nearly ideal response. Figure 9 depicts the ideal shear, bending moment, and torque influence coefficient plots.

Influence coefficients for an elevated temperature calibration were calculated, and these values compared to influence coefficients obtained from a room temperature calibration (ref. 6). Influence coefficients for six bending bridges and six shear bridges are shown in figures 10 and 11. These data show similar trends for both room temperature and elevated temperature conditions, but the value of the influence coefficients and their slopes differ slightly between the two load calibrations. Slight differences are expected because nonuniform elastic modulus degradation with temperature would result in (1) generally increased strain levels to compensate for generally decreased elastic modulus values and (2) a nominal amount of increased strain values resulting from load path changes. The gage factor of the strain gages changes with temperature, and finally, the beaded panels deform as a result of the changing thermal conditions.

Load Equation Accuracy

The derived equation coefficients β_i, used to calculate the loads, are shown in tables 3 and 4. Table 3 lists coefficients for the room temperature equations, and table 4 lists coefficients for elevated temperature equations.

The plots of figure 8 show the difference in standard error between room temperature equations and elevated temperature equations. The shear equations show that room temperature equations containing from 12 to 6 bridges have a smaller standard error than the elevated temperature equations. The 5-bridge equation has the same standard error, while the 4-bridge, 3-bridge, and 2-bridge equations show a smaller stan-

dard error for the elevated temperature equations. In the case of the bending equations (fig. 8(b)), there is a smaller standard error for room temperature equations from 12 to 3 bridges, with the elevated temperature equation showing less error for the 2-bridge equation. The torque equations in figure 8(c) show a smaller standard error for the room temperature equations in all cases.

To assess the ability of the equations to calculate loads applied to the structure, a load distribution was applied to the structure that was independent of the point-by-point calibration loading. This check loading was applied after the test structure had been stabilized at the elevated temperature. The distributed loading is depicted in figure 12 and represents a midplanform center of pressure.

As the structure was heated, thermal stresses caused the strain gage bridges to produce outputs. The value of this output at elevated temperature with no load applied to the structure is called thermal shift. These thermal shifts are subtracted from the bridge output at load and temperature to obtain the true output due to load only. These true values are then entered in the room temperature and elevated temperature equations to produce the calculated loads.

The thermal stresses measured in this test were small because loading was performed at quasi-equilibrium temperatures and the design of the test article minimized thermal stress. The thermal shift in thermal outputs of the strain gage bridges may be significantly higher for dynamic temperature distributions and other structural designs.

The results of the multiple-point check loading (distributed load) are shown in figure 13. This figure shows that in most cases the equations derived using room temperature loading produce results that are closer in value to the actual applied load than the loads calculated using the elevated temperature equations. The exceptions are the 4-bridge, 5-bridge, and 6-bridge bending-moment equations. In these cases the elevated temperature equations show only a few percent improvement. Also shown in figure 13 is the increased deviation from applied load when the thermal shift is not used to correct the strain gage outputs at elevated temperature.

The difference in the results for the room temperature equations and the elevated temperature equations is of little practical significance. Hence, it must be concluded that the room temperature load calibration can be used satisfactorily at elevated temperature for this structure.

Load Equation Influence Coefficients

Influence coefficients for complete load equations were computed using the method in reference 8. These are shown as equation influence coefficient plots in figures 14 to 16. The perfect shear expression would appear as a horizontal line, with all chord lines falling on top of each other, indicating no response to bending or torsion. A perfect bending response would be a straight, sloping line passing through the origin with all chord lines falling on top of each other. A perfect torsion equation would have an influence coefficient plot that possesses the same shape as the planform of the constant chord lines. As can be seen from the equation coefficient plots, the deviation from the ideal situation increases as the number of strain gage bridges in the equation is reduced.

CONCLUDING REMARKS

A strain gage load calibration was conducted on a representative part of a wing structure designed for high-temperature flight applications. Load equations were derived from a high-temperature load calibration, and these load equations were compared to load equations derived from a room temperature calibration on the same structure. The implications of the high-temperature load calibration were studied from the viewpoint of applicability and necessity.

Load equations derived from the room temperature load calibration resulted in generally lower equation standard errors than equations derived from the elevated temperature load calibration. A distributed load was applied to the structure at elevated temperature and strain gage outputs were measured to assess whether it is necessary to calibrate this structure at elevated temperature. The applied load was then calculated with equations derived from both the room temperature and elevated temperature calibration data. It was found that no significant differences between the two equation systems existed in terms of computing this applied distributed load, as long as the thermal shifts are taken into account. The identification of these thermal shifts requires that the structure be heated. Therefore, for this structure, a high-

temperature load calibration is not required; however, a heating of the structure is required to determine thermal shifts.

Ames Research Center
Dryden Flight Research Facility
National Aeronautics and Space Administration
Edwards, California, April 30, 1987

REFERENCES

1. Skopinski, T.H.; Aiken, William S., Jr.; and Huston, Wilbur B.: Calibration of Strain-Gage Installations in Aircraft Structures for Measurement of Flight Loads. NACA Report 1178, 1954.

2. Plank, P.P. and Penning, F.A.: Hypersonic Wing Test Structure Design, Analysis, and Fabrication. NASA CR-127490, 1973.

3. Sefic, Walter J.: NASA Dryden Flight Loads Research Facility. NASA TM-81368, 1981.

4. Fields, Roger A.; Reardon, Lawrence F.; and Siegel, William H.: Loading Tests of a Wing Structure for Hypersonic Aircraft. NASA TP-1596, 1980.

5. Tang, Ming H. and Sheldon, Robert G.: A Modified T-Value Method for Selection of Strain Gages for Measuring Loads on a Low Aspect Ratio Wing. NASA TP-1748, 1980.

6. Sefic, Walter J. and Reardon, Lawrence F.: Loads Calibration of the Airplane. NASA YF-12 Loads Program, NASA TM X-3061, 1974, pp. 61–107. (C)

7. Hovell, P.B.; Roberts, T.A.; and Webber, D.A.: The Use of Calibrated Strain Gauges for Flight Load Determination, CP-1041, British A.R.C., 1969.

8. Jenkins, Jerald M.; Kuhl, Albert E.; and Carter, Alan L.: Strain Gage Calibration of a Complex Wing, AIAA J. Aircraft, vol. 14, no. 12, December 1977, pp. 1192–1196.

TABLE 1. MAXIMUM TEMPERATURES AT STRAIN GAGE LOCATIONS

	Strain gage bridge number											
	104	105	304	305	504	505	704	705	904	905	1104	1105
Location	Strain gage bridge temperatures, °F											
Upper bending bridge	388		471		487		484		480		372	
Lower bending bridge	341		446		464		439		439		331	
Shear bridge		374		437		460		464		435		352

TABLE 2. HWTS STRAIN GAGE CALIBRATION LOAD SCHEDULE
(2000 lb/load point)

Test number	Run number	Load point
1	1	1
	2	3
	3	5
	4	7
	5	9
	6	11
	7	13
	8	15
	9	16
	10	17
2	11	2
	12	4
	13	6
	14	8
	15	10
	16	12
	17	14
	18	16
3	(Check load)	1 to 18

TABLE 3. LOAD EQUATION COEFFICIENTS DERIVED FROM ROOM TEMPERATURE DATA

(a) Coefficients for measuring shear

Strain gage bridge number	Number of strain gage bridges										
	12	11	10	9	8	7	6	5	4	3	2
	Shear, lb/μ										
104	2.75	2.65	4.11	3.82	3.06	—	—	—	—	—	—
105	7.41	7.46	7.26	7.20	7.42	8.96	11.24	11.44	13.75	19.57	17.32
304	3.12	4.25	—	—	—	—	—	—	—	—	—
305	6.97	6.72	7.58	7.55	6.68	5.82	—	—	—	—	—
504	2.72	—	—	—	—	—	—	—	—	—	—
505	7.58	8.12	7.83	7.92	11.30	10.73	14.65	13.11	—	–	—
704	4.10	5.22	7.74	9.34	12.23	19.27	18.87	15.27	15.61	—	—
705	7.27	6.87	6.28	5.82	—	—	—	—	—	—	—
904	4.08	4.56	4.52	—	—	—	—	—	—	—	—
905	6.54	6.48	6.68	7.85	10.76	10.38	9.87	15.11	19.48	18.49	—
1104	3.54	3.48	3.57	5.86	5.79	4.91	5.54	9.07	9.42	14.21	15.20
1105	6.78	6.82	6.77	5.94	5.44	5.97	5.83	—	—	—	—

TABLE 3. CONTINUED.

(b) Coefficients for measuring bending moment

Strain gage bridge number	Number of strain gage bridges										
	12	11	10	9	8	7	6	5	4	3	2
	Bending moment, in.-lb/μ										
104	417.70	401.11	350.84	323.74	334.58	324.14	—	—	—	—	—
105	-76.60	-62.89	—	—	—	—	—	—	—	—	—
304	561.54	631.44	675.90	860.74	829.24	1004.86	1672.59	2048.09	1963.71	1822.05	1929.59
305	-92.37	-150.25	-219.13	-272.74	-250.49	-247.62	-299.40	-317.70	-321.80	—	—
504	523.68	429.36	449.91	478.31	454.46	—	—	—	—	—	—
505	-91.99	—	—	—	—	—	—	—	—	—	—
704	763.82	801.64	800.87	549.89	601.38	768.51	676.77	—	—	—	—
705	-137.35	-191.91	-167.11	—	—	—	—	—	—	—	—
904	841.64	851.39	869.43	954.32	1155.10	1239.27	1095.02	1468.10	2054.75	2147.25	2005.41
905	-220.63	-214.98	-223.18	-343.13	-455.16	-475.01	-439.19	-431.28	-463.96	-501.12	—
1104	591.88	592.61	592.11	542.66	389.59	383.92	391.18	279.87	—	—	—
1105	-161.11	-158.72	-155.16	-117.02	—	—	—	—	—	—	—

TABLE 3. CONCLUDED.

(c) Coefficients for measuring torque

Strain gage bridge number	Number of strain gage bridges										
	12	11	10	9	8	7	6	5	4	3	2
	Torque, in.-lb/μ										
104	-172.19	-169.61	-146.59	-94.00	—	—	—	—	—	—	—
105	103.21	102.83	102.21	—	—	—	—	—	—	—	—
304	8.43	—	—	—	—	—	—	—	—	—	—
305	269.69	271.43	269.24	394.25	366.89	440.70	564.07	569.89	560.18	—	—
504	216.14	219.23	—	—	—	—	—	—	—	—	—
505	419.32	418.23	455.29	401.23	417.26	318.87	—	—	—	—	—
704	396.69	399.67	544.01	470.38	192.26	—	—	—	—	—	—
705	571.75	571.20	526.83	538.20	597.05	685.75	899.90	952.34	1078.51	1394.65	—
904	621.83	621.23	659.58	632.48	776.78	1094.67	1003.64	1789.40	1744.82	1834.00	1944.57
905	601.54	601.93	601.74	604.59	556.85	510.73	474.29	173.03	—	—	—
1104	640.97	641.20	638.10	635.16	602.18	492.38	528.91	—	—	—	—
1105	817.21	817.08	819.49	814.00	827.13	812.14	823.21	1109.61	1173.46	977.73	1091.89

TABLE 4. LOAD EQUATION COEFFICIENTS DERIVED FROM ELEVATED TEMPERATURE DATA

(a) Coefficients for measuring shear

Strain gage bridge number	Number of strain gage bridges										
	12	11	10	9	8	7	6	5	4	3	2
	Torque, in.-lb/μ										
104	0.23	—	—	—	—	—	—	—	—	—	—
105	8.33	8.39	8.30	7.98	8.12	10.19	10.12	11.18	16.43	18.47	17.52
304	7.35	8.02	7.92	14.20	13.22	12.62	13.10	9.34	—	—	—
305	5.26	5.14	5.18	5.17	5.69	—	—	—	—	—	
504	1.60	1.31	—	—	—	—	—	—	—	—	—
505	8.97	9.02	9.24	9.08	9.02	13.70	16.35	14.89	14.39	—	—
704	7.07	7.09	8.58	—	—	—	—	—	—	—	—
705	5.39	5.42	4.73	6.53	7.08	4.98	—	—	—	—	—
904	-3.91	-4.04	-4.53	-4.38	—	—	—	—	—	—	—
905	9.32	9.34	9.88	9.69	8.56	9.75	12.47	16.71	14.81	18.54	—
1104	7.68	7.74	8.21	8.56	5.60	6.77	7.00	10.02	12.97	13.04	14.31
1105	5.57	5.55	5.11	4.53	6.23	4.98	4.59	—	—	—	—

TABLE 4. CONTINUED.

(b) Coefficients for measuring bending

Strain gage bridge number	Number of strain gage bridges										
	12	11	10	9	8	7	6	5	4	3	2
	Bending, lbs-in.										
104	151.78	159.99	184.39	140.57	95.68	116.88	—	—	—	—	—
105	44.83	35.60	—	—	—	—	—	—	—	—	—
304	888.48	866.93	834.47	949.00	1119.29	1015.03	1424.69	1309.63	1193.34	1671.07	2419.24
305	-264.93	-229.20	-191.38	-191.13	-199.96	-168.23	-184.40	-157.77	—	—	—
504	164.80	199.97	193.38	—	—	—	—	—	—	—	—
505	58.21	—	—	—	—	—	—	—	—	—	—
704	1440.21	1406.92	1425.62	1585.85	1502.48	1522.38	1320.87	1555.16	1629.41	962.82	—
705	-373.45	-327.23	-346.30	-392.87	-272.00	-286.47	-234.58	-321.91	-380.95	—	—
904	-180.11	-165.29	-171.68	247.09	-180.87	—	—	—	—	—	—
905	133.30	110.98	115.25	169.52	—	—	—	—	—	—	—
1104	1100.16	1084.06	1079.20	1138.25	1044.67	937.38	897.30	838.00	858.32	863.01	890.26
1105	-242.58	-229.17	-229.24	-276.64	-171.18	-126.92	-90.42	—	—	—	—

TABLE 4. CONCLUDED.

(c) Coefficients for measuring torque

Strain gage bridge number	Number of strain gage bridges										
	12	11	10	9	8	7	6	5	4	3	2
	Torque, lbs-in.										
104	-276.36	-259.12	-242.42	-245.67	-184.54	-213.77	-29.02	–	–	–	–
105	123.49	120.90	121.83	125.44	–	–	–	–	–	–	–
304	75.21	–	–	–	–	–	–	–	–	–	–
305	300.82	309.50	314.43	327.54	489.01	647.53	653.54	633.26	606.67	–	–
504	-185.94	-166.08	–	–	–	–	–	–	–	–	–
505	462.06	458.44	429.97	428.22	351.14	–	–	–	–	–	–
704	987.48	1017.78	806.46	779.25	724.10	720.57	–	–	–	–	–
705	398.98	391.02	473.56	496.37	520.30	760.71	816.43	801.62	1353.78	1667.85	1877.29
904	-196.36	-185.76	-124.43	–	–	–	–	–	–	–	–
905	905.87	906.43	843.08	808.51	782.31	713.44	858.79	843.54	–	–	–
1104	1055.90	1050.99	995.85	911.27	867.41	857.93	1060.61	1043.29	916.12	958.43	1379.16
1105	713.14	714.64	763.15	811.79	836.66	853.86	598.40	627.55	920.46	728.01	–

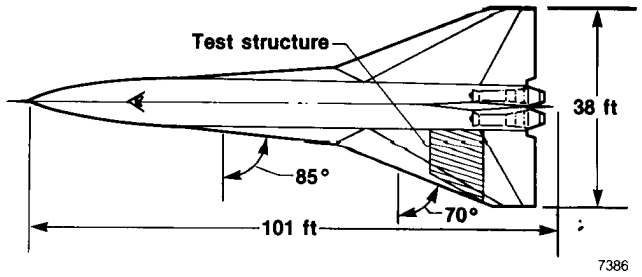

Figure 1. High-speed airplane and wing test structure.

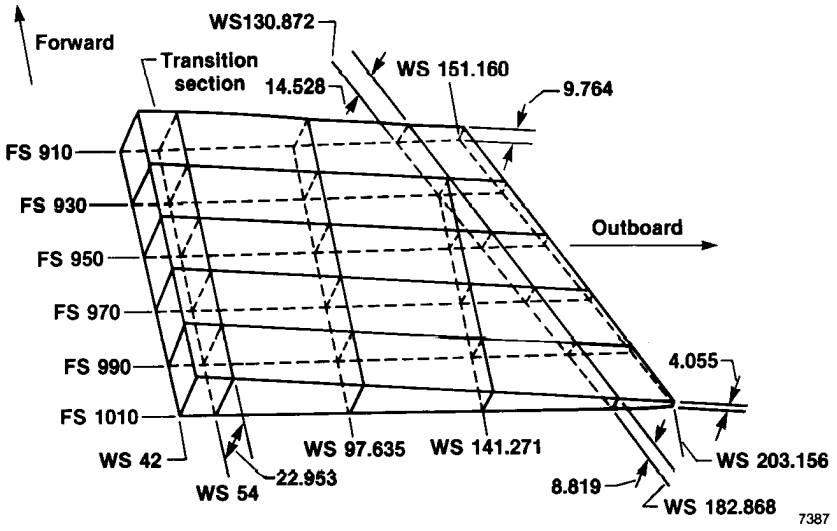

Figure 2. Test structure dimensions. Fuselage stations, wing stations (WS), inches.

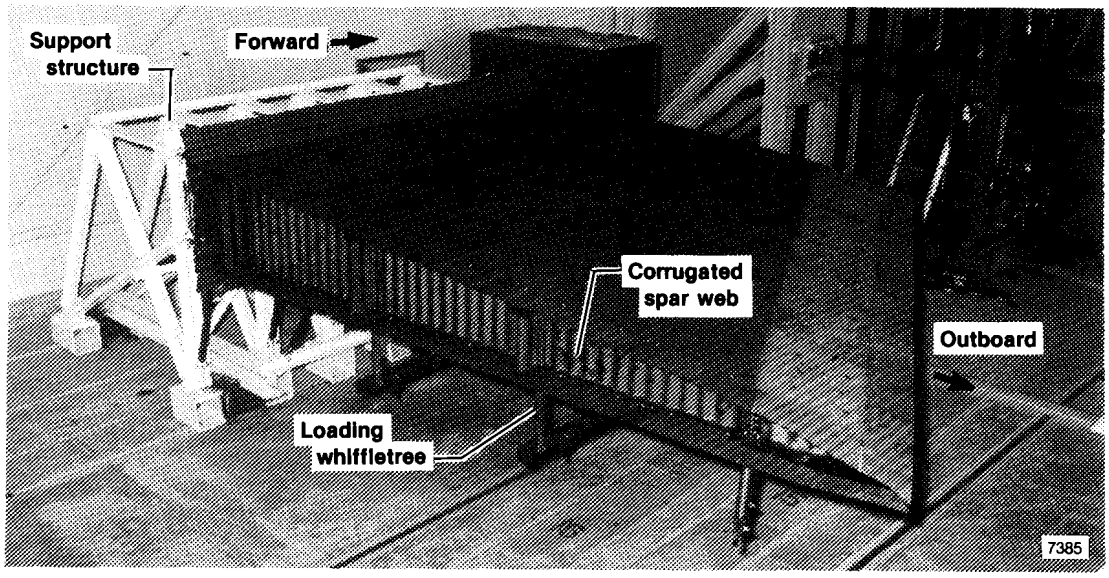

E 26145

Figure 3. Test structure with heat shields installed.

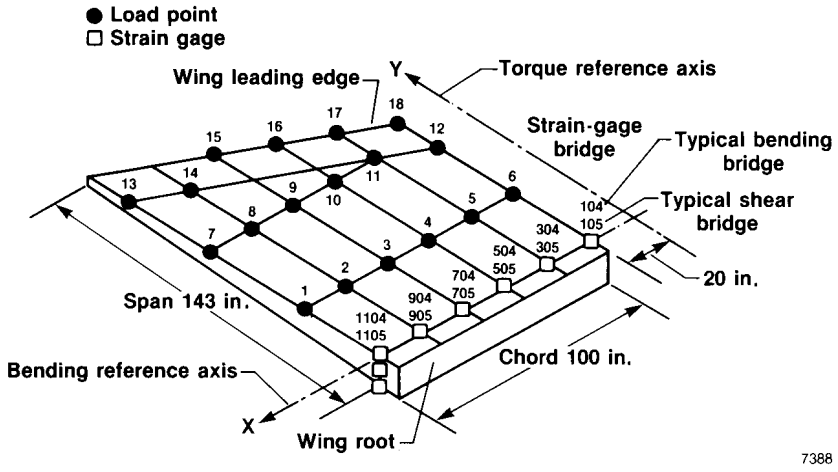

Figure 4. Strain gage bridge locations and calibration load points on the test structure. Wing is shown inverted from the test position.

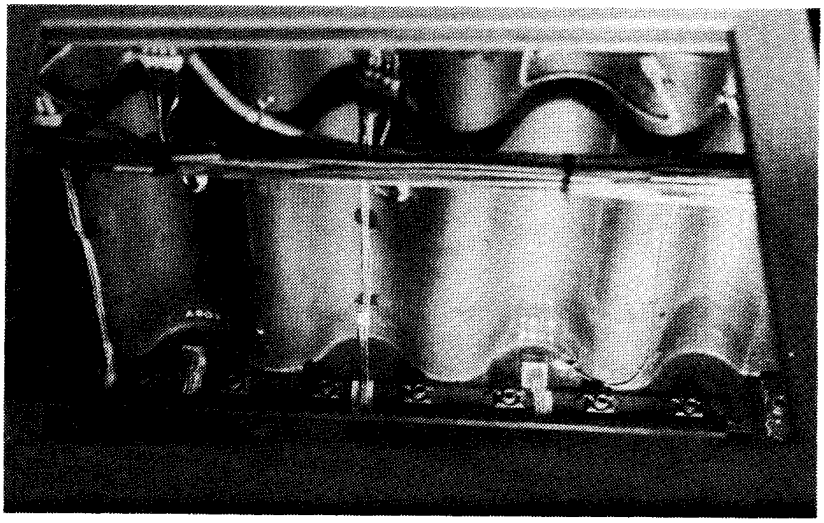

E 27930

(a) Bending strain gage bridge.

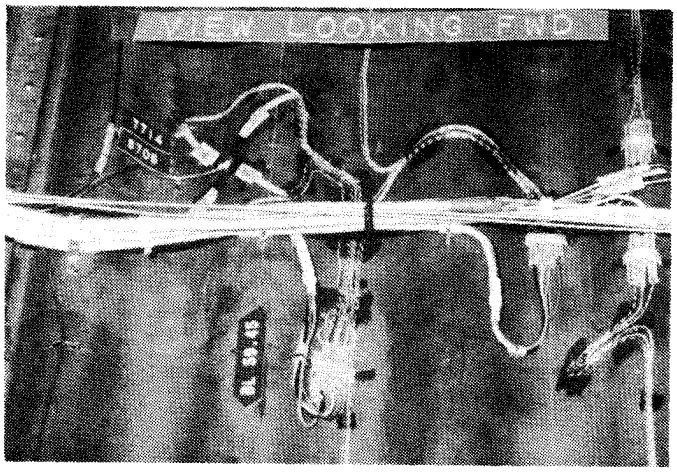

E 27928

(b) Shear strain gage bridge.

Figure 5. Bending and shear strain gage bridges on the test structure.

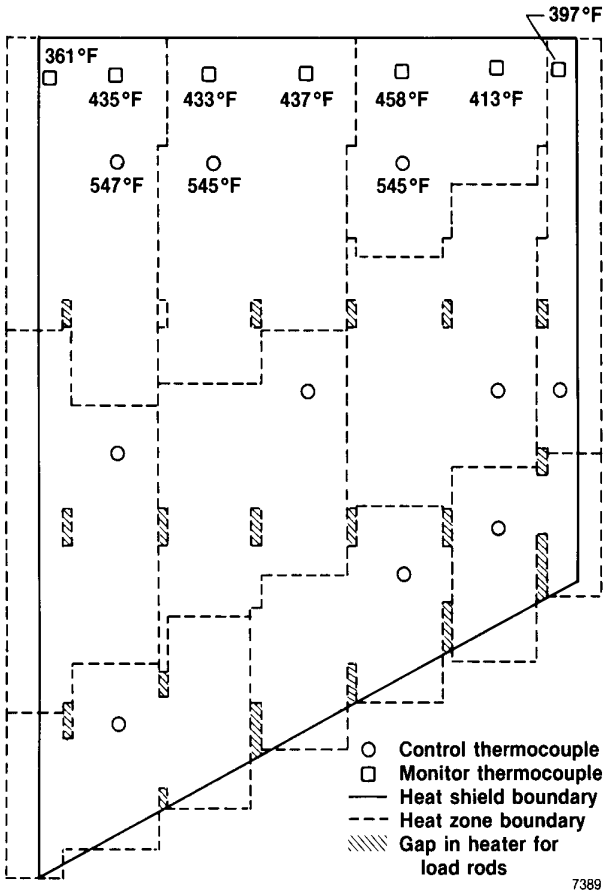

(a) Lower surface heater.

Figure 6. Heating zones for test structure.

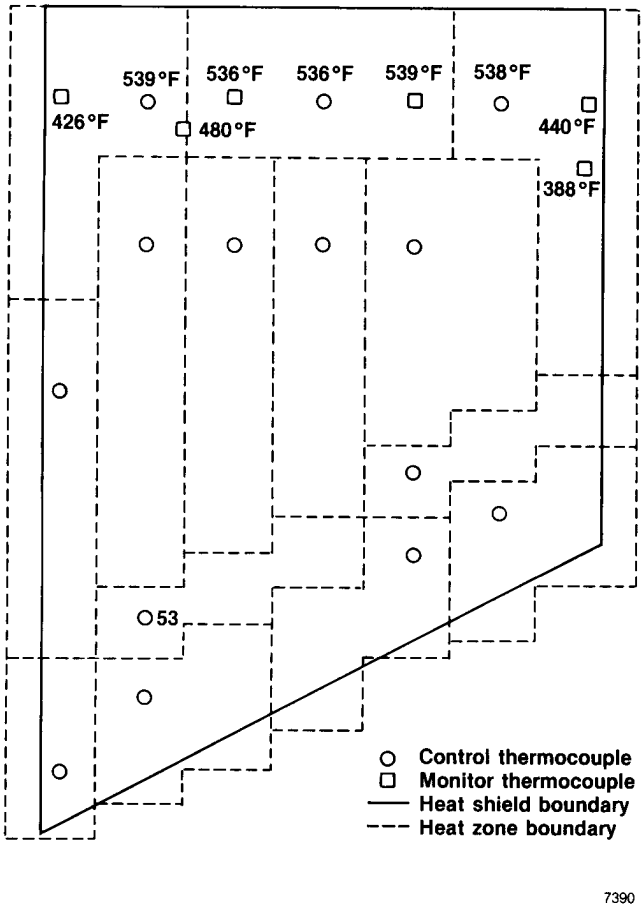

(b) Upper surface heater.

Figure 6. Concluded.

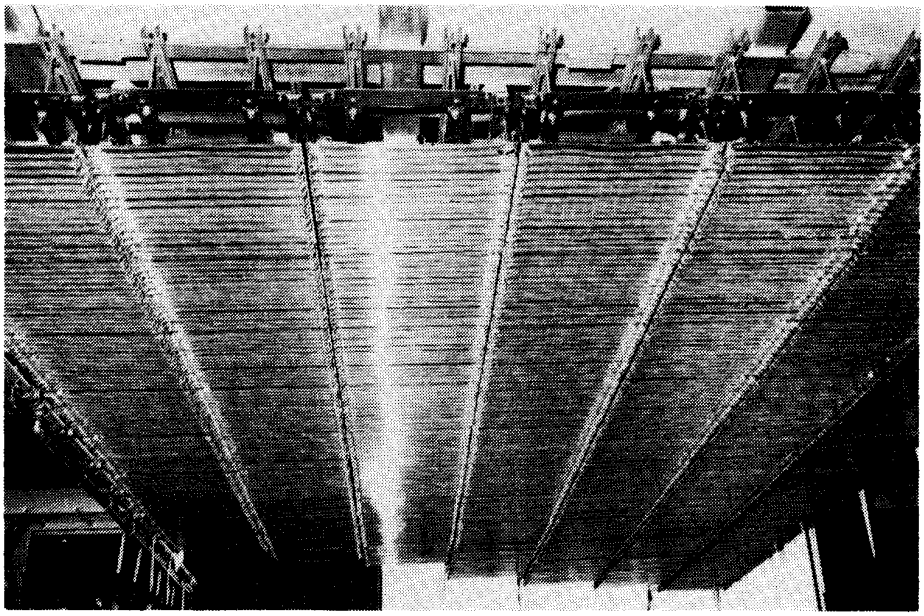

E 31078

(a) Upper reflector.

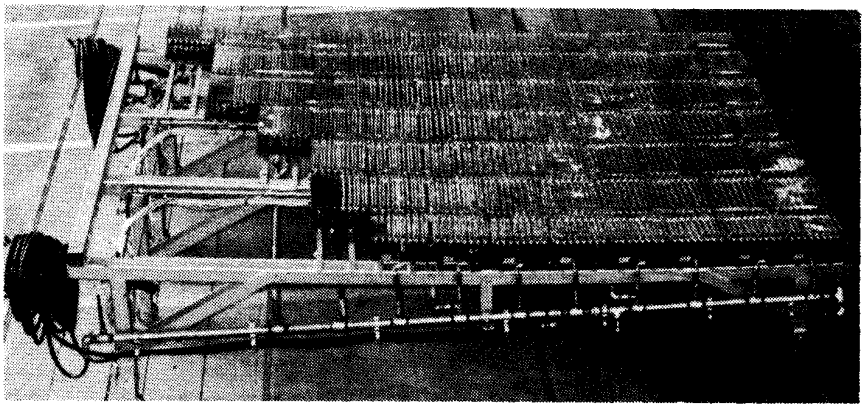

E 31077

(b) Lower reflector.

Figure 7. Water-cooled reflectors.

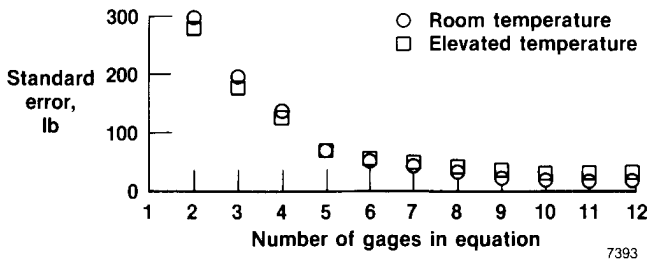

(a) Shear equations.

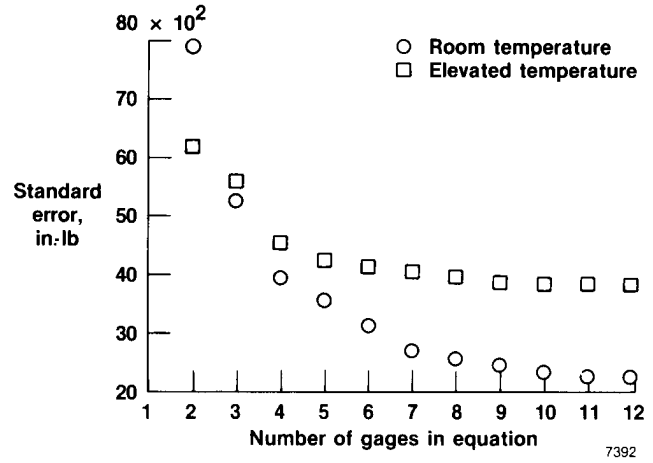

(b) Bending equations.

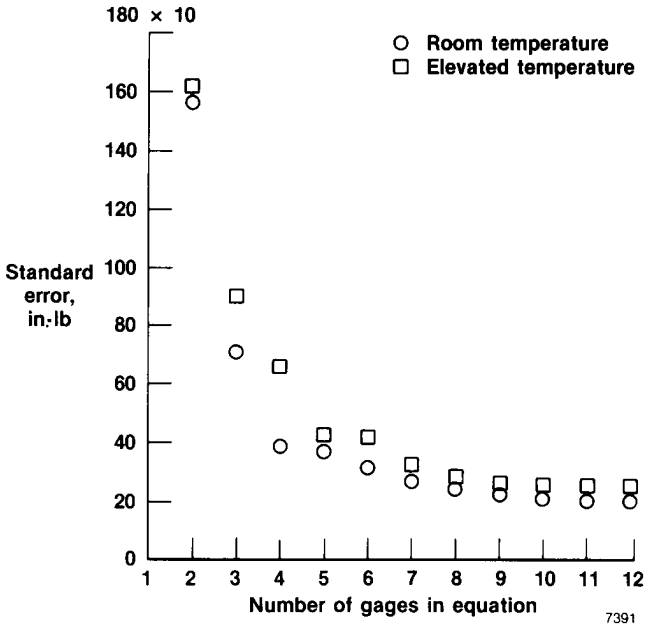

(c) Torque equations.

Figure 8. Load equation errors as a function of the number of strain gage bridges in each equation.

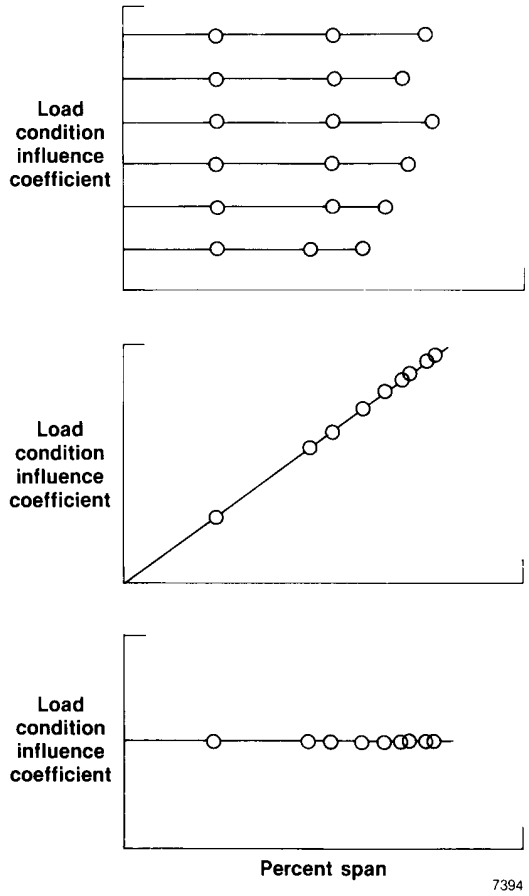

Figure 9. Ideal strain gage bridge influence coefficient plots.

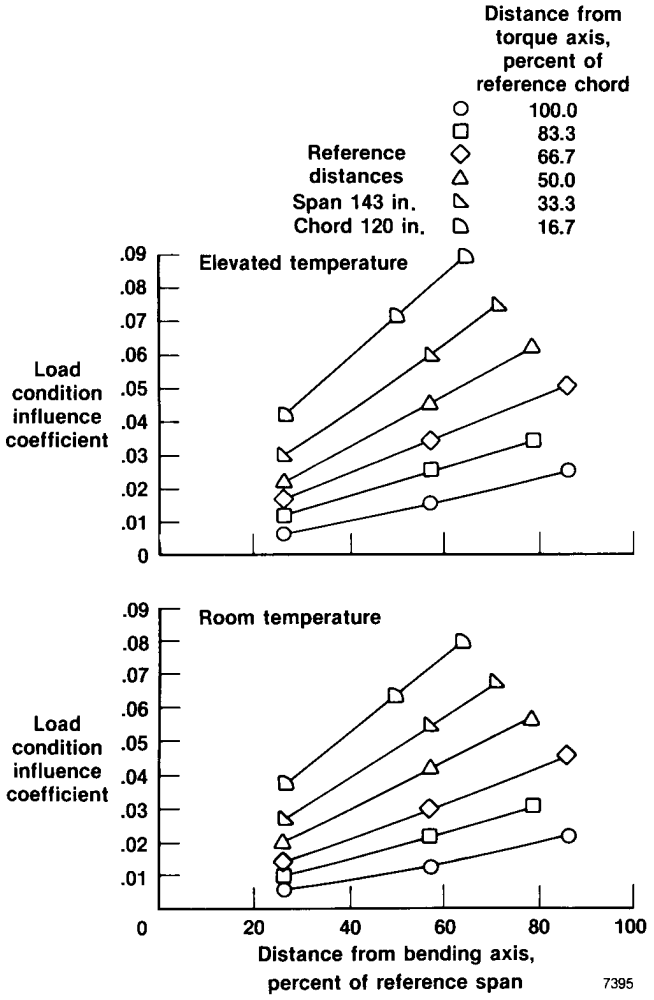

(a) Bridge 104.

Figure 10. Strain gage bending bridge influence coefficients.

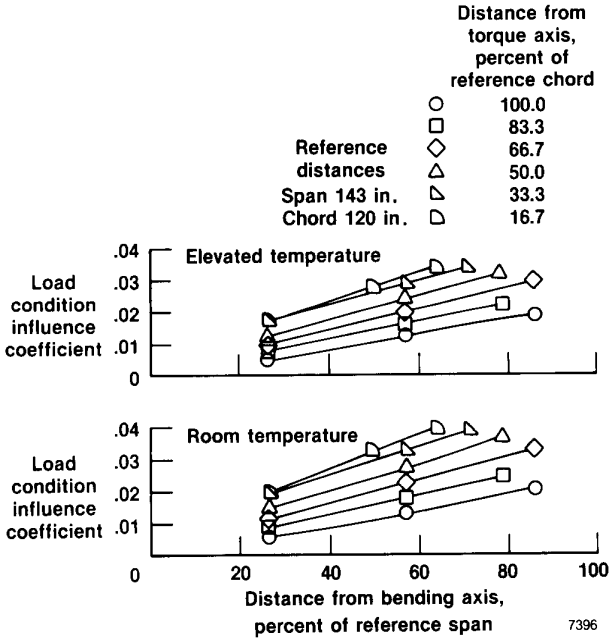

(b) Bridge 304.

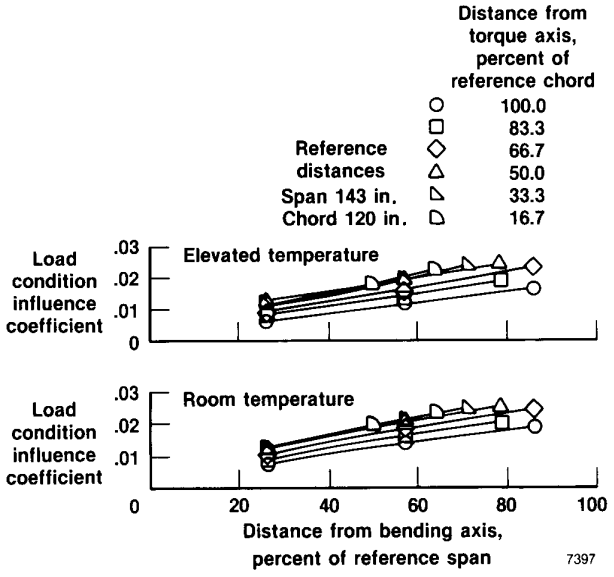

(c) Bridge 504.

Figure 10. Continued.

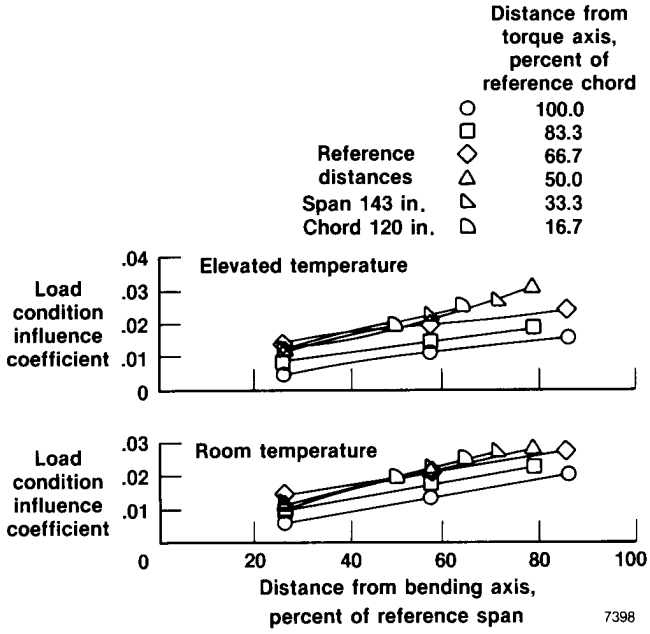

(d) Bridge 704.

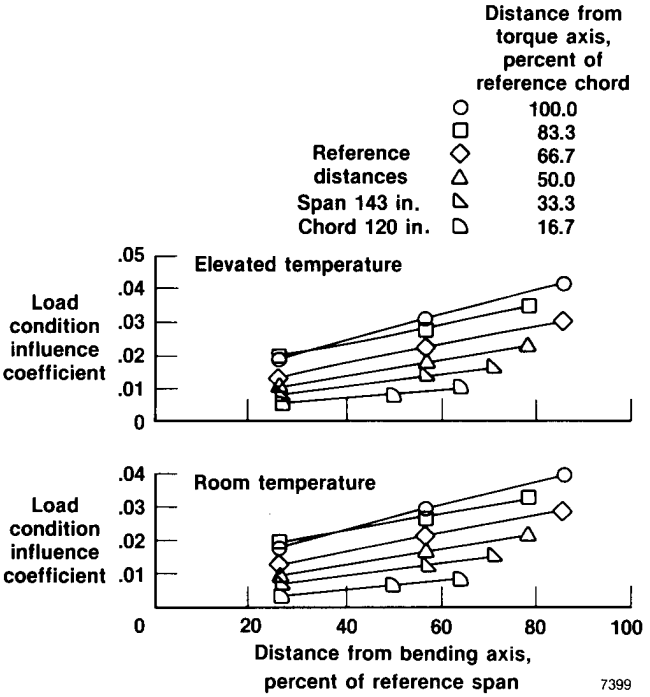

(e) Bridge 904.

Figure 10. Continued.

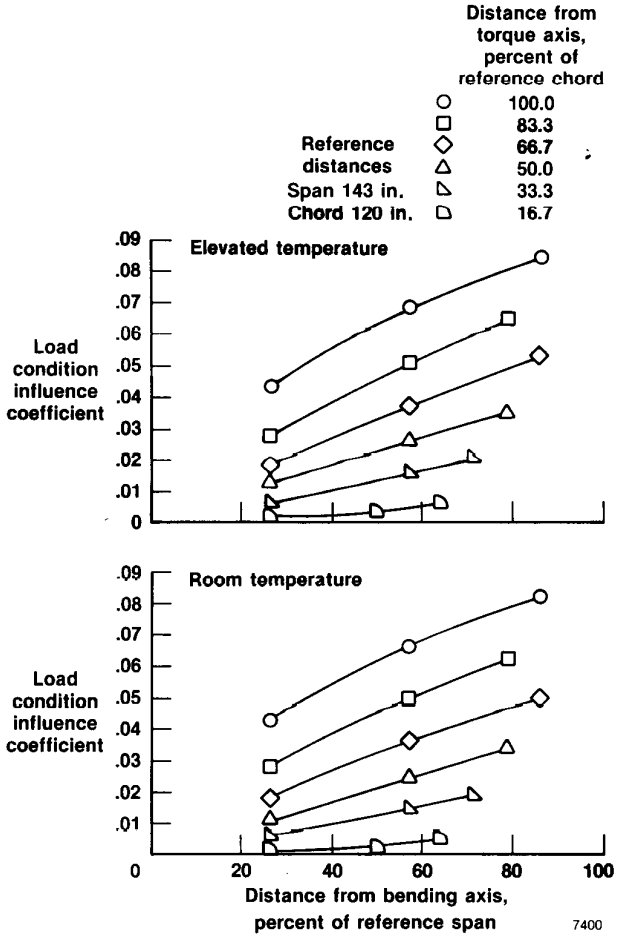

(f) Bridge 1104.

Figure 10. Concluded.

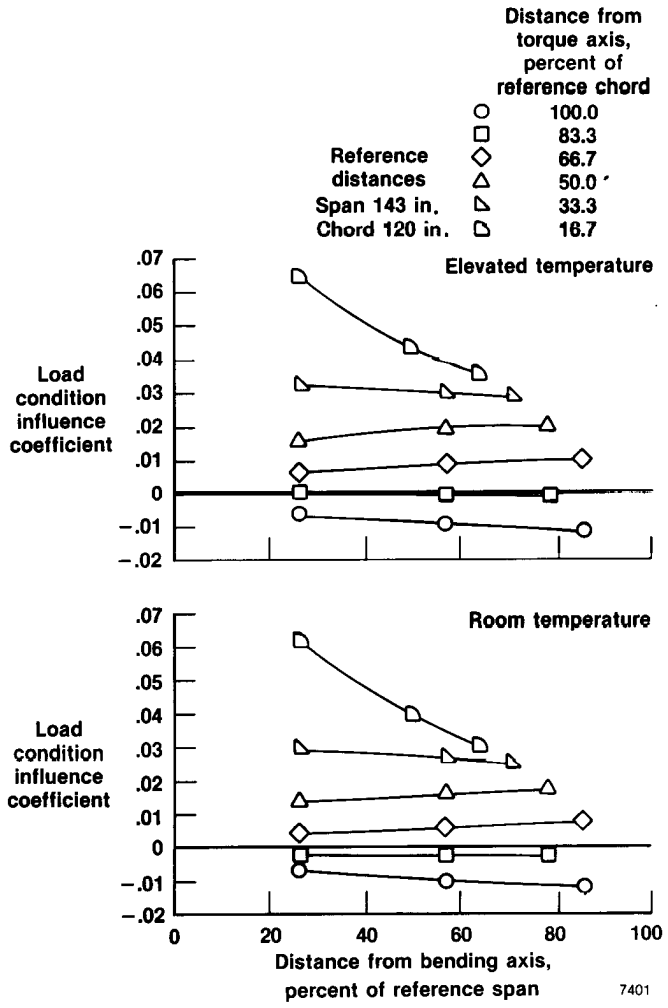

(a) Bridge 105.

Figure 11. Strain gage shear bridge influence coefficients.

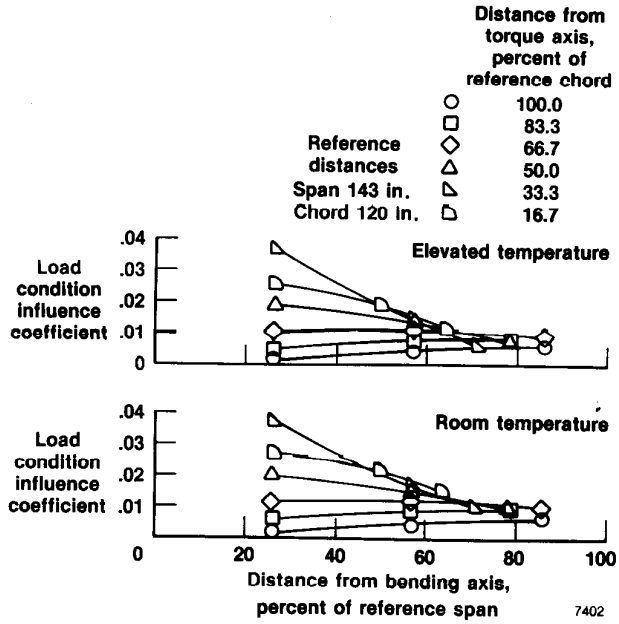

(b) Bridge 305.

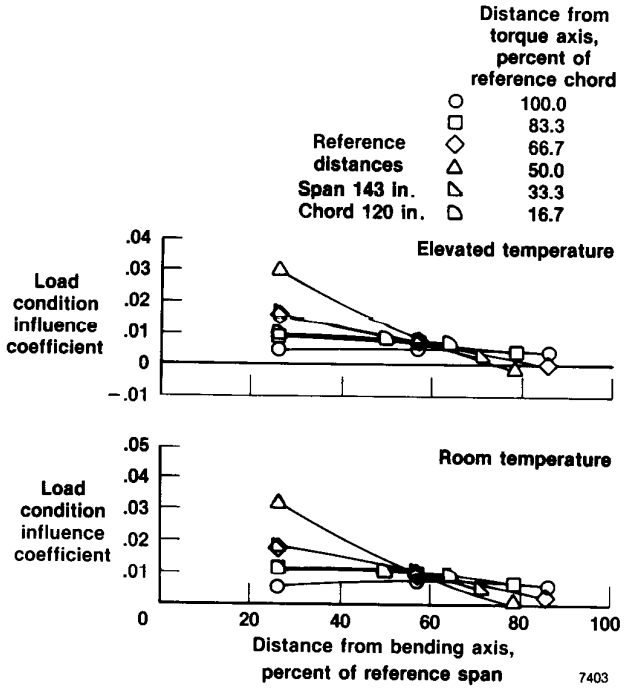

(c) Bridge 505.

Figure 11. Continued.

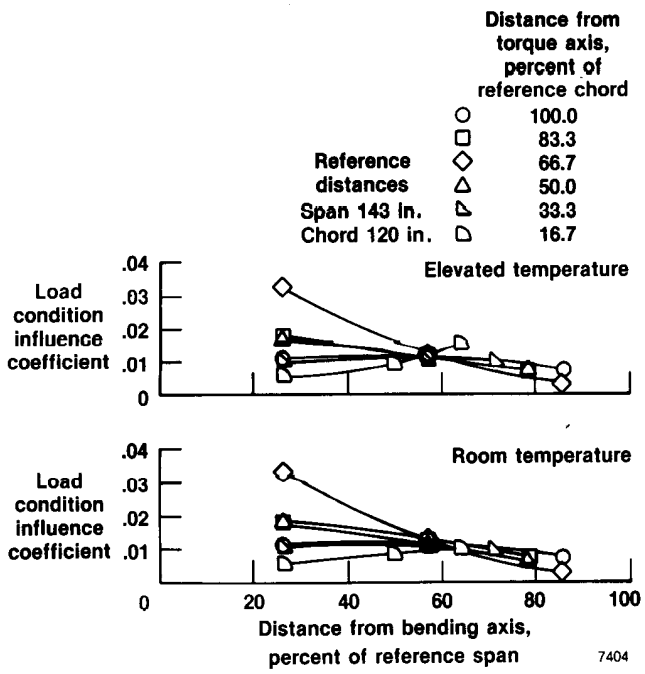

(d) Bridge 705.

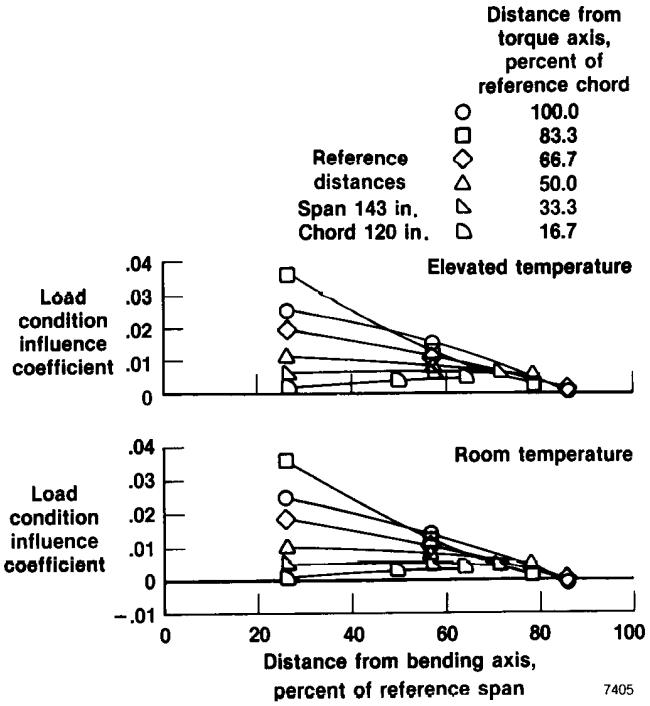

(e) Bridge 905.

Figure 11. Continued.

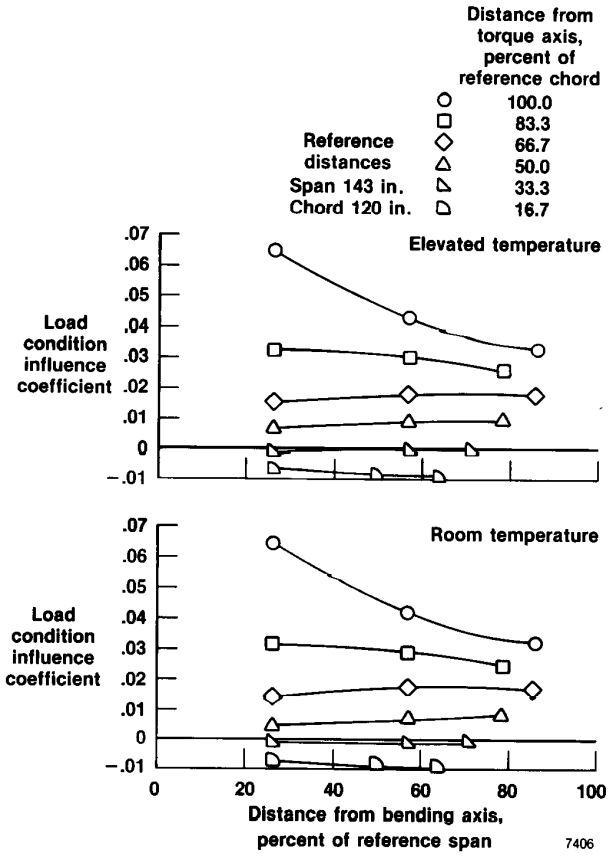

(f) Bridge 1105.

Figure 11. Concluded.

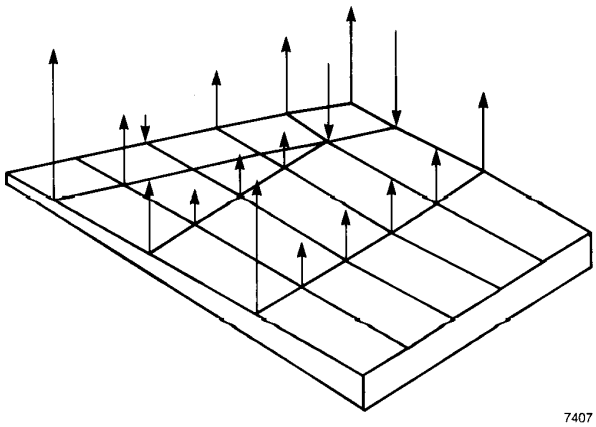

Figure 12. Shear loads applied with midcenter of pressure. View of test structure lower surface.

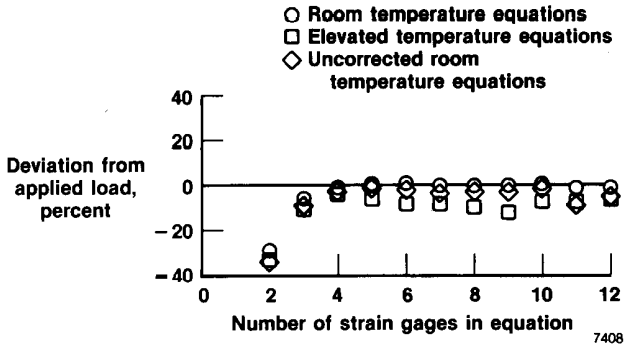

(a) Shear.

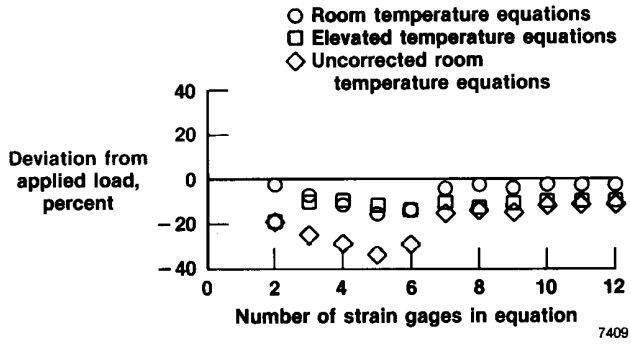

(b) Bending.

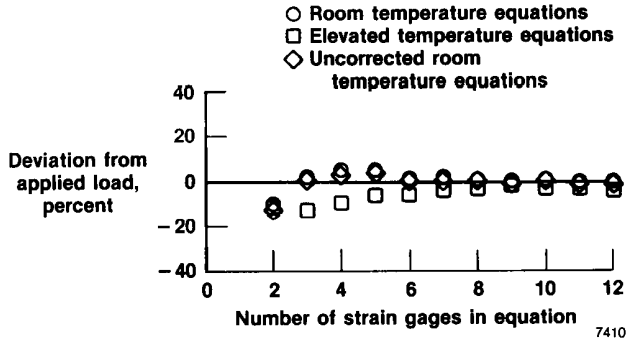

(c) Torque.

Figure 13. Comparison of loads computed with room temperature and elevated temperature equations.

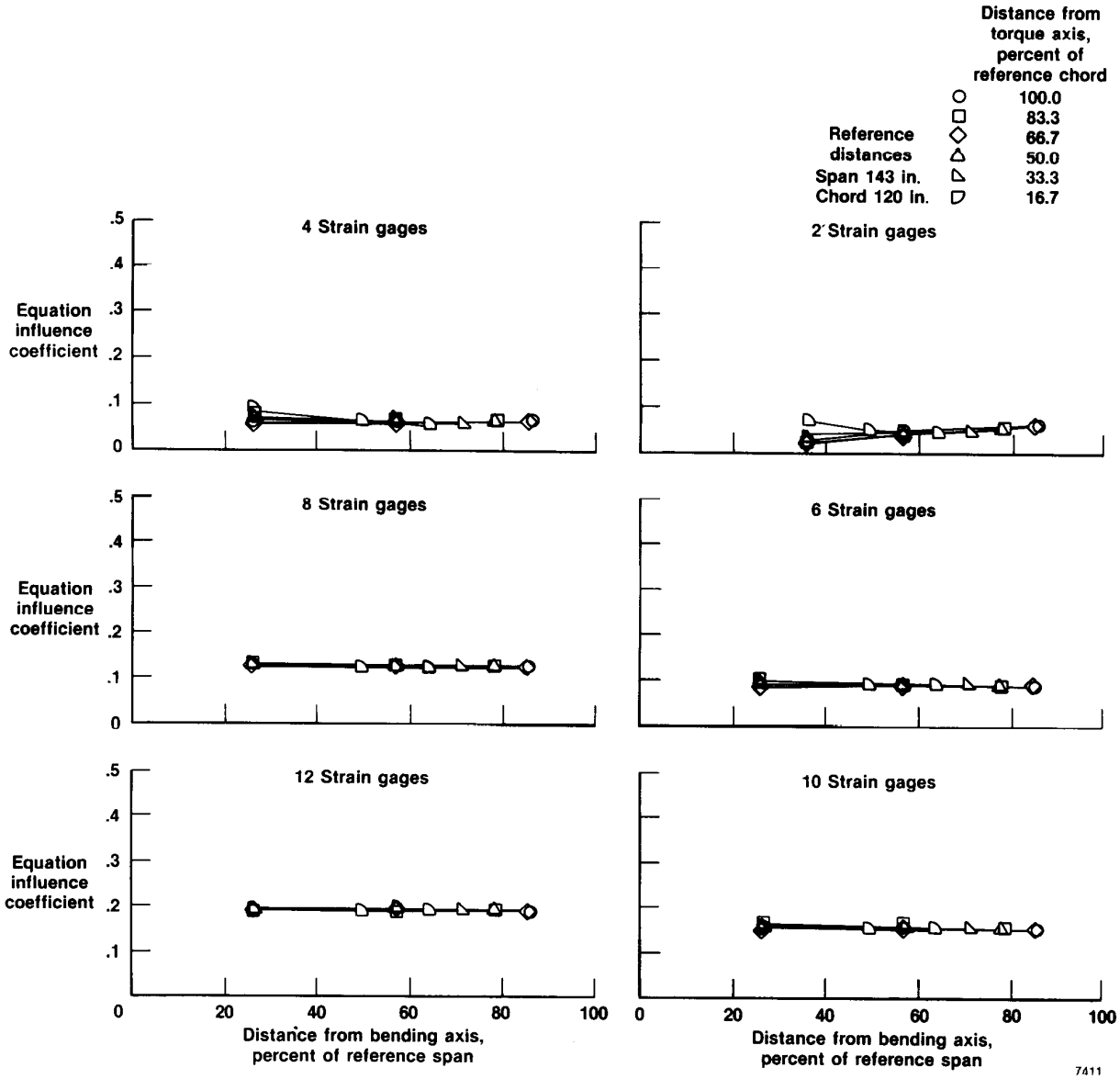

(a) Elevated temperature.

Figure 14. Computed shear equation influence coefficients.

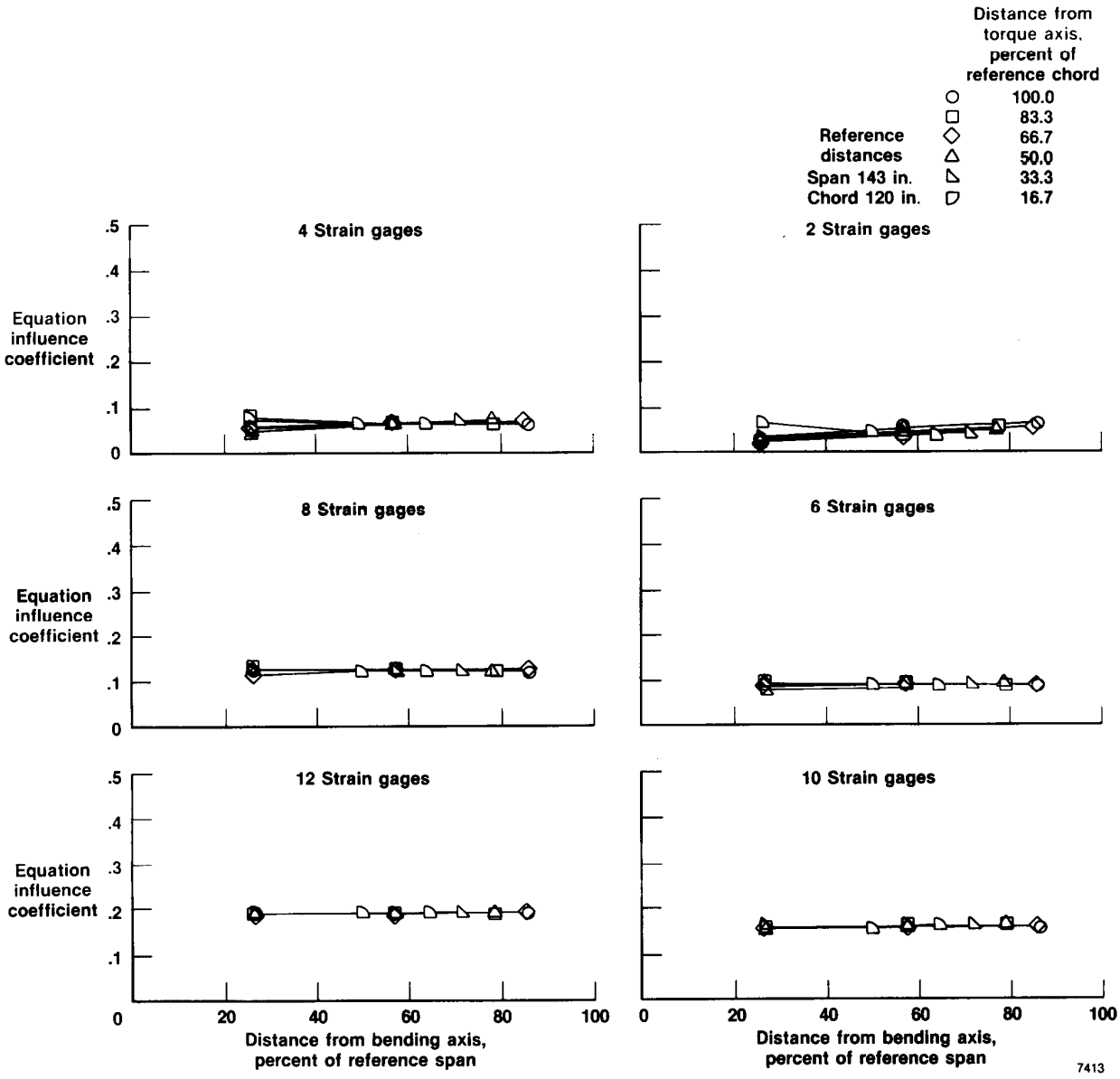

(b) Room temperature.

Figure 14. Concluded.

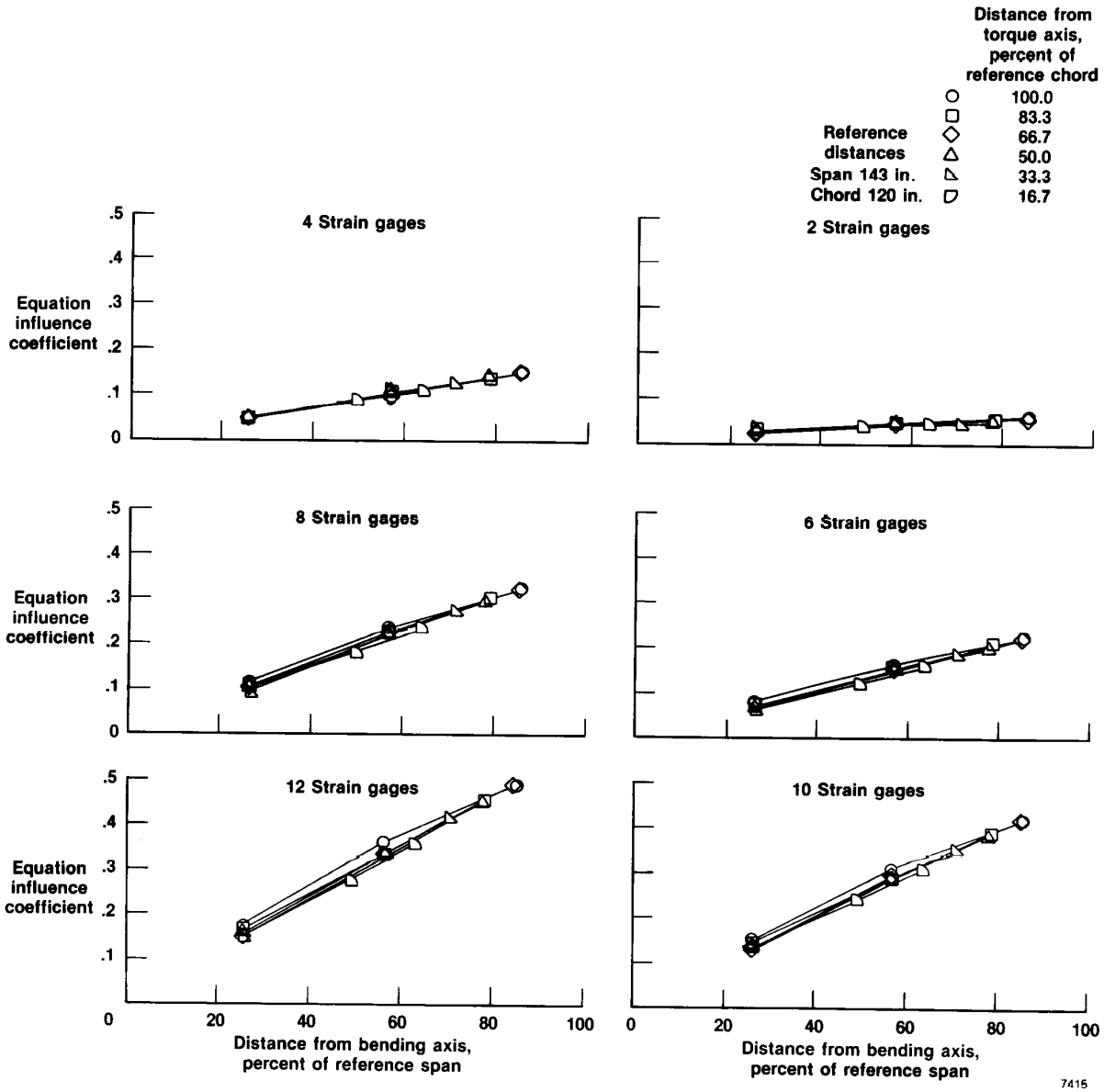

(a) Elevated temperature.

Figure 15. Computed bending equation influence coefficients.

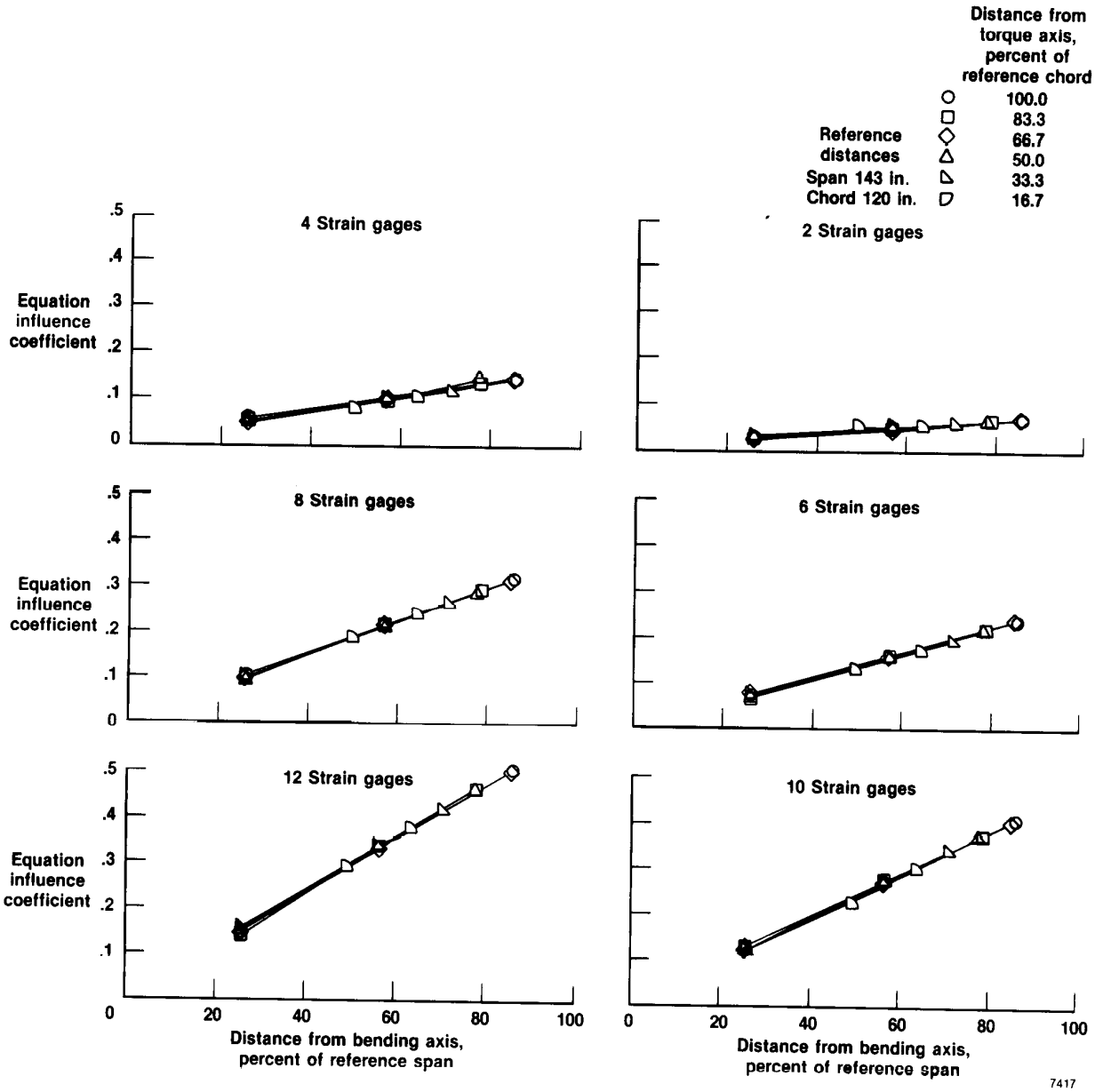

(b) Room temperature.

Figure 15. Concluded.

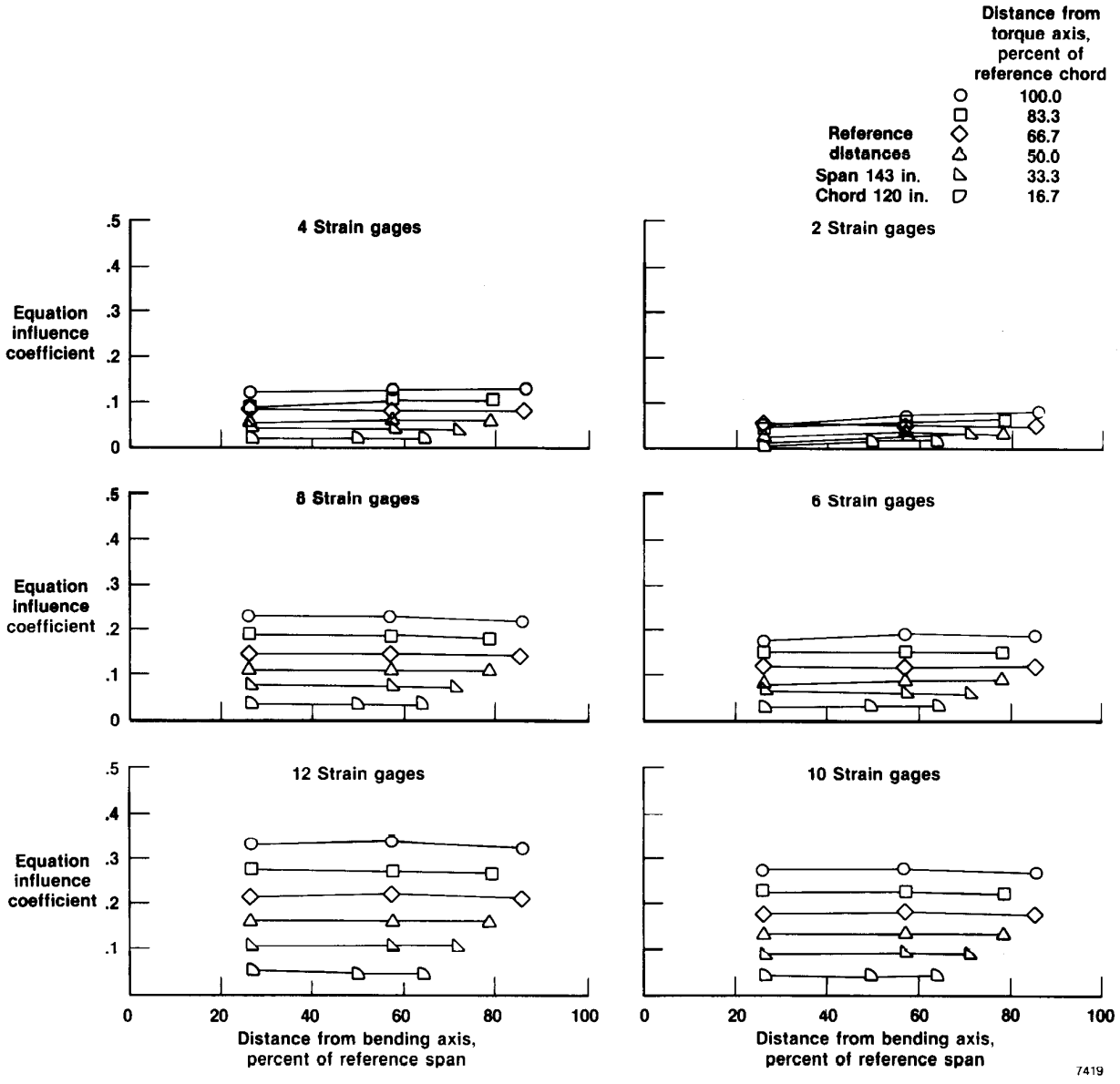

(a) Elevated temperature.

Figure 16. Computed torque equation influence coefficients.

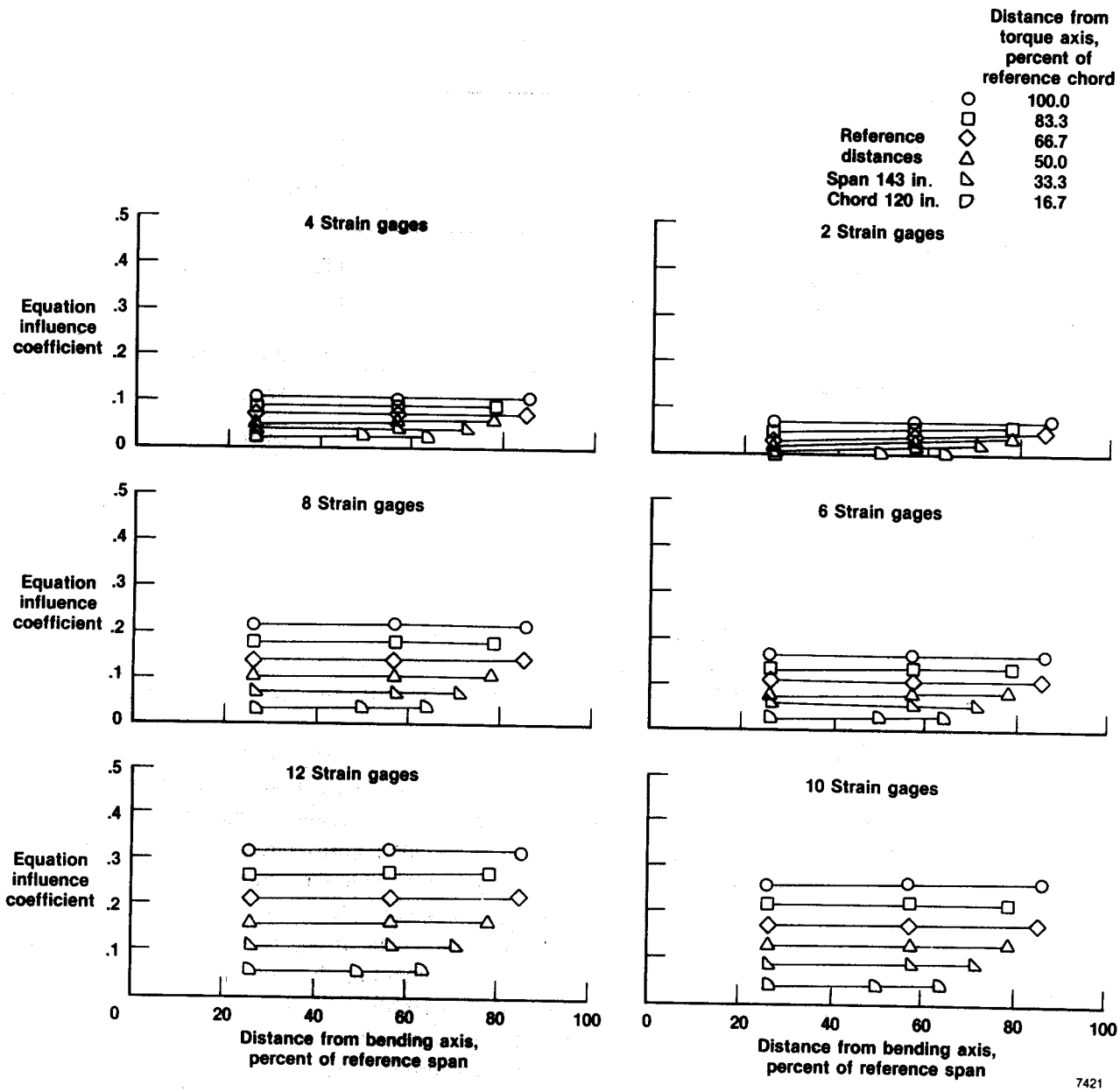

(b) Room temperature.

Figure 16. Concluded.

NASA National Aeronautics and Space Administration

Report Documentation Page

1. Report No.	2. Government Accession No.	3. Recipient's Catalog No.
NASA TP-2921		

4. Title and Subtitle

Evaluation of a Strain-Gage Load Calibration on a Low-Aspect-Ratio Wing Structure at Elevated Temperature

5. Report Date

June 1989

6. Performing Organization Code

7. Author(s)

Lawrence F. Reardon

8. Performing Organization Report No.

H-1331

10. Work Unit No.

RTOP 506-43-81

9. Performing Organization Name and Address

NASA Ames Research Center
Dryden Flight Research Facility
P.O. Box 273, Edwards, CA 93523-5000

11. Contract or Grant No.

13. Type of Report and Period Covered

Technical Paper

12. Sponsoring Agency Name and Address

National Aeronautics and Space Administration
Washington, DC 20546

14. Sponsoring Agency Code

15. Supplementary Notes

16. Abstract

This report addresses the environmental aspect of elevated temperature and how it relates to the science of strain gage calibrations of aircraft structures. A section of a wing designed for a high-speed aircraft structure was used to study this problem. This structure was instrumented with strain gages calibrated at both elevated and room temperatures.

Load equations derived from a high-temperature load calibration were compared with equations derived from an identical load calibration at room temperature. The implications of the high temperature load calibration were studied from the viewpoint of applicability and necessity. Load equations derived from the room temperature load calibration resulted in generally lower equation standard errors than equations derived from the elevated temperature load calibration. A distributed load was applied to the structure at elevated temperature and strain gage outputs were measured. This applied load was then calculated using equations derived from both the room temperature and elevated temperature calibration data. It was found that no significant differences between the two equation systems existed in terms of computing this applied distributed load, as long as the thermal shifts resulting from thermal stresses could be identified. This identification requires a heating of the structure. Therefore, it is concluded that for this structure, a high temperature load calibration is not required, however, a heating of the structure is required to determine thermal shifts.

17. Key Words (Suggested by Author(s))	18. Distribution Statement
Calibration Elevated temperature Hypersonic wing test structure Strain gage	Unclassified — Unlimited Subject category 39

19. Security Classif. (of this report)	20. Security Classif. (of this page)	21. No. of pages	22. Price
Unclassified	Unclassified	39	A03

NASA FORM 1626 OCT 86

For sale by the National Technical Information Service, Springfield, VA 22161-2171.

NASA-Langley, 1989